

Origin of the Counterintuitive Dynamic Charge in the Transition-Metal Dichalcogenides

Nicholas A. Pike,^{1,2,*} Benoit Van Troeye,^{2,3} Antoine Dewandre,^{1,2} Xavier Gonze,^{2,3} and Matthieu J. Verstraete^{1,2}

¹*Université de Liège, CESAM Physique des Matériaux et Nanostructures, B-4000 Liège, Belgium*

²*The European Theoretical Spectroscopy Facility (www.etsf.eu)*

³*Université Catholique de Louvain, Institute of Condensed Matter and Nanosciences (IMCN), B-1348 Louvain-la-Neuve, Belgium*

(Dated: March 29, 2022)

We investigate the chemical bonding characteristics of the transition-metal dichalcogenides thanks to an analysis of the static and dynamical charges within the Density Functional Theory framework. The dynamical charges of the trigonal transition-metal dichalcogenides are found anomalous, while in their hexagonal counterparts, the sign of the dynamic charge is counterintuitive i.e. the transition-metal takes the negative dynamic charge. Here we show that this phenomena cannot be understood by analysis of the static charges and present our theoretical understanding of this phenomena based on the perturbative response of the system to a static electric field and by investigating the hybridization of the molecular-orbitals near the Fermi level. Furthermore, we establish a link between the sign of the Born effective charge and the hybridization of the molecular-orbitals near the Fermi level and propose an experimental procedure to verify the calculated sign of the dynamical charge in the transition-metal dichalcogenides.

PACS numbers: Density Functional Theory +GGA
Van der Waals Interaction
Transition-metal Dichalcogenides

The expanding interest in the Transition-Metal Dichalcogenides (TMDs) stems from their wide variety of applications, ranging from batteries to electronic devices [1, 2]. Indeed, by adjusting either their chemical composition or the number of layers, one can tune their electronic, vibrational, and magnetic properties in a manner irreproducible by other two-dimensional and layered materials. In particular, the TMDs offer high carrier mobilities [3–5] and a strain-dependent indirect to direct band gap transition [6], that are crucial for future electronic and electro-optic applications [2, 7, 8]. Still, while the electronic properties of these materials are now relatively well-known [9], the character of their chemical bonds is, to the best of our knowledge, not yet fully-understood. For example, while ZrS₂ is reported as extremely ionic [12], MoS₂ and WS₂ are reported to possess both ionic and covalent characteristics [13, 14]. Additionally, TiS₂ was recently reported as metallic and semiconducting, both experimentally and theoretically [15–17].

In this letter, we aim to provide a deeper understanding of the bonding characteristics and charge transfer in the TMDs thanks to Density Functional Theory (DFT) [18]. One common way to estimate the static charge within this theory is to arbitrarily partition the electronic density of the system into constituent atoms [19, 20]. While conceptually simple, this notion of “static” charge is unfortunately ambiguous [21] and the corresponding charges cannot be measured experimentally. Contrarily, the dynamical charge, arising from the change of dipole moment due to an atomic perturbation, i.e. the Born effective charge (BEC) [22] is a physical observable as it governs, for example, the splitting between

the transverse optical (TO) and longitudinal optical (LO) vibrational modes [22].

In this paper, we highlight the critical differences between the dynamical BECs and static Bader charges in the cases of the hexagonal TMDs (h-TMDs). Indeed, our BEC calculations indicate that the transition-metal atom takes the negative charge, while the nominal and computed static charges leads to the opposite conclusion. This contrasts strongly with the case of the trigonal TMDs (t-TMDs) for which we find that the sign of the Bader charge and BEC agree. In what follows, we discuss these fundamental discrepancies, and more importantly, explain the origin of the counterintuitive sign of the BECs in the h-TMDs by investigating the localization of the hybridized molecular-orbitals near the Fermi level. We propose finally an experimental method to verify our theoretical observations.

Our calculations are performed using the *Abinit* software package [23–25] with the GGA-PBE exchange-correlation functional [18, 26, 27], corrected by Grimme’s DFT-D3 functional for the dispersion corrections due to long range electron-electron correlations [28, 29]. With the inclusion of this functional, we are able to reproduce the in-plane and out-of-plane experimental lattice parameters within 0.7% [30–35]. Details on the norm-conserving pseudopotentials, the convergence parameters (plane-wave expansion cutoff energy and Brillouin-zone sampling) and the structural parameters is found in the Supplemental Material [36]. We investigate the Bader charge, Z^B , and BEC, Z^* , for the bulk MX₂ h-TMDs, where M= Mo, W and X= S, Se, Te, as well as for TiS₂ and TiSe₂, two semiconducting t-TMDs. We use Den-

h-TMD	Born effective charge [e]				Static Dynamical	
	This work		Exp. 39-42		Bader [e]	
	$Z_{\text{Mo},xx}^*$	$Z_{\text{Mo},zz}^*$	$ Z_{\text{Mo},xx}^* $	$ Z_{\text{Mo},zz}^* $	Z_{Mo}^B	$Z_{\text{Mo},z}^{B,*}$
MoS ₂	-1.090	-0.628	1.11	0.4	1.155	0.635
MoSe ₂	-1.904	-0.952	2.1	0.5	0.910	0.652
MoTe ₂	-3.280	-1.562	3.4		0.575	0.752
WS ₂	-0.505	-0.426	0.45	0.2	1.400	
WSe ₂	-1.242	-0.776	1.7	0.5	1.081	
t-TMD						
TiS ₂	6.344	1.208	8.3	2.2	1.764	1.330
TiSe ₂	8.230	1.092	9.2	2.1	1.599	

TABLE I. Computed BECs, static Bader charge, and dynamic Bader charge for the transition metal atom in the h-TMDs and t-TMDs. The dynamic Bader charge is defined below. The BECs and Bader charges for the chalcogen atoms is exactly opposite and half the corresponding transition-metal charge. The absolute value of the experimental BECs is also reported.

sity Functional Perturbation Theory (DFPT) [22, 37, 38] to calculate the BECs with the charge neutrality condition imposed. All calculations of the static and dynamic charges use the relaxed geometries for the individual compounds.

In Table I, we report our calculated BECs and Bader charges for the previously introduced TMDs, alongside experimental data extracted from infrared spectra [39–42] which only provides a measure of the magnitude of the BEC. In terms of the magnitude of the BEC, our calculated BECs agree quantitatively with the experiments. However, for the studied t-TMDs, the BECs are found anomalous as they differ strongly from both their corresponding nominal and static charges. Moreover, we observe that the dynamical charges in h-TMDs are counterintuitive, with the transition-metal and chalcogen atoms taking the negative and positive charges, respectively, in disagreement with the corresponding nominal and static charges. These counterintuitive BECs for h-TMDs were also observed recently [43], even for monolayer TMDs, although the authors did not remark upon, or provide an explanation for the calculated sign. In the following, we will first discuss the discrepancies observed between the static and dynamical charges in the h-TMDs, before explaining the physical origin of the counterintuitive sign of the BECs.

As mentioned previously, the static and dynamical charges cannot be directly compared due to the differences in the methods of calculation. Namely, the static charge being calculated from a ground-state density partition and the dynamic charge being calculated as a response function. Still, one can construct a dynamical charge based on the static charge, by taking into account of the change of Bader charge with an atomic displacement [21] computed by finite differences. This newly-constructed dynamical charge, denoted $Z^{B,*}$ in-

cludes additional effects i.e. the charge localization and delocalization but fails to account for the local change in polarization around the atoms. To avoid the creation of an electron current, which cannot be quantified by our approach, we only consider atomic displacements in the out-plane direction. The corresponding charges are reported in Tab. I. While these dynamical charges are in better agreement with our computed BECs, the additional contribution is found to be too small to explain fully the sign of the BECs in h-TMDs. We understand this in terms of a local change of polarization around the atoms that cannot be quantified by such an approach [21]. This is furthermore confirmed by the analysis of the perturbed density with an atomic displacement, presented in Fig. (S2) of the supplemental material [36], that is localized closely to the Mo atoms (a region that cannot be described by Bader as discussed in the supplemental material [36]).

Consequently, the analysis of the BECs is crucial to understanding the discrepancies in dynamical charges between h-TMDs and t-TMDs. We focus in the following on MoS₂ and TiS₂. The band-by-band decomposition [44] and localization tensor [45] are unable to bring any simple nor conclusive explanations on the difference of BECs between these two materials as shown in Table (S3) in the supplemental material. [36]. Thus, it is necessary to analyze the different contributions to the BECs which are given explicitly, for example, in Ref. 22. Neglecting the separable part, the BEC can be expressed in terms of two contributions; the first one, the ionic charge of the system, is static and always positive for the transition-metal atom. The second contribution, the dynamic correction corresponding to the effects of electronic screening, is responsible for the sign change observed here. A detailed discussion of these two terms is found in the supplementary material [36].

The dynamic screening component, given in Eq. (S3) of the supplemental material [36], depends explicitly on, first, the change in the electronic wavefunction due to an electric field perturbation and, second, the change of electronic potential due to an atomic displacement. While the change in potential does not vary qualitatively between MoS₂ and TiS₂ (see Fig. S2) [36], their first-order density responses differ significantly, as illustrated in Fig. 1. In MoS₂, this change of electronic density with an external electric field is localized around the Mo atom (Fig. 1b), while, in TiS₂, it is delocalized along the Ti-S bond (Fig. 1e).

As a consequence of this localization, the dynamic response to an electric field is directly related to the orbital hybridization of the h-TMDs. With this in mind, and in order to understand the fundamental differences in the orbital hybridization in MoS₂ and TiS₂, we show a Molecular Orbital (MO) diagram [46] based on the previous work of Stiefel *et al.* [47]. Similar to their work, we write down the molecular orbitals of MoS₂ and TiS₂ molecules

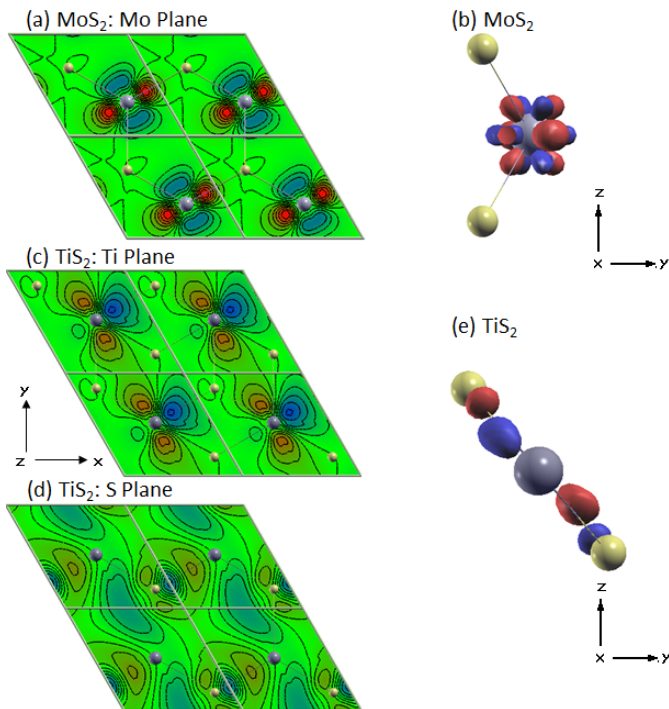


FIG. 1. (Color Online) Contour plots and isosurfaces of the change in the electronic density due to an electric field perturbation along the x axis for MoS_2 and TiS_2 . For MoS_2 we show, (a) a contour plot of the in-plane change in the electronic density around a Mo-atom and (b) the isosurface of the induced change in the electronic density for a single formula unit of MoS_2 . The change in the electronic density around S is negligible (not presented). For TiS_2 we show the contour plots of the in-plane change in electronic density around (c) Ti and (d) S, as well as (e) the isosurface of the induced change in the electronic density for a single formula unit of TiS_2 . Blue, red and green indicate positive, negative, negligible changes in the electronic density. The atomic colors indicate the transition-metal, in gray, and the chalcogen atom, in tan.

using the irreducible representation of the molecular orbitals for a single formula unit within these compounds. Therefore, we use the point group symmetries D_{3h} and D_{3d} , for MoS_2 and TiS_2 , respectively. By looking at the MO diagrams at Γ we can understand the origin of the sign of the BEC thanks to a direct comparison to the projected orbital analysis of the MoS_2 and TiS_2 calculations presented in the supplementary material [36].

The MO diagram for the MoS_2 molecule in D_{3h} symmetry is presented in Fig. 2. It indicates that the lowest A'_1 , as well as the lowest E' and E'' molecular orbitals of MoS_2 are all bonding orbitals. According to the projected orbital analysis, the A'_1 is mostly of S character, while the E' and E'' share both Mo and S orbital characters. The A'_2 orbital, arising from the interaction between p_z orbitals of S, does not hybridizing with the Mo atomic orbitals.

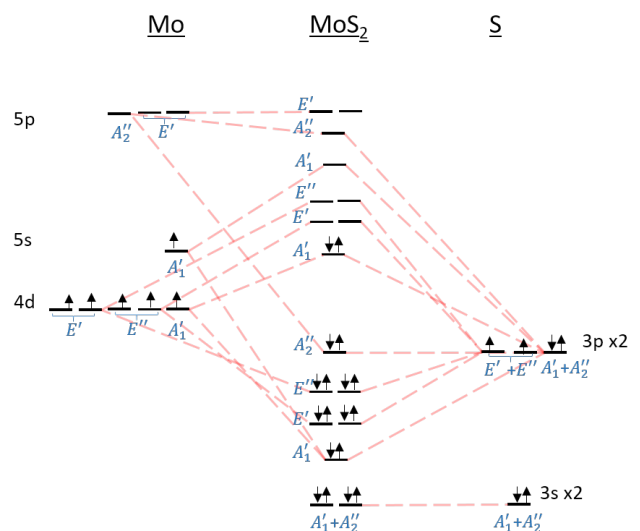


FIG. 2. (Color Online) Molecular orbital diagram of MoS_2 . The symmetry notation, in blue, labels the symmetry type of the molecular orbital and the light red dashed lines are the symbolic links between the atomic and molecular orbitals.

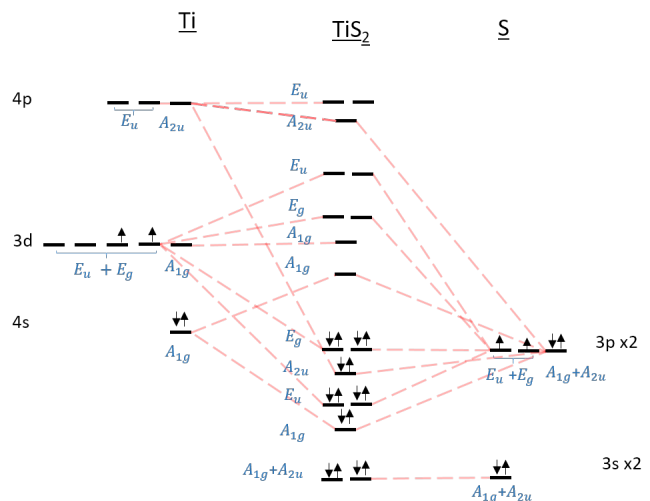


FIG. 3. (Color Online) Molecular orbital diagram of TiS_2 . The symmetry notation, in blue, labels the symmetry type of the molecular orbital and the light red dashed lines are the symbolic links between the atomic and molecular orbitals.

The last occupied orbital, the anti-bonding A'_1 orbital, lies nearest the Fermi energy of our system and contributes most strongly to the transfer of charge upon movement of the transition-metal ion. Our analysis of the projected orbital band structure at the equilibrium position of the atoms, found in the supplementary material [36], confirms that the highest occupied A'_1 mode is composed primarily of atomic orbitals from the Mo atom, the lower A'_1 band is primarily S in nature, and the occupied A'_2 is of S character.

Upon displacement of the Mo atom, the highest occupied A'_1 MO will transfer charge back to the Mo 4d states. It is this transfer which is responsible for the sign of the BEC and the π back-bonding. Additionally, the increase in the magnitude of the BEC as a function of the chalcogen (S, Se, Te), seen in Table I, can be understood in terms of the increased weight of transition-metal atomic orbitals in this MO as shown in Fig. (S5) of the supplemental material [36]. Additionally, the ordering and bonding characteristics of the h-TMDs are remarkably different from those of the t-TMDs as shown in Fig. 3. Here we show the MO diagram of TiS_2 using the notation of the D_{3d} point group. In particular, we find that all the valence bands of TiS_2 should contain a majority of atomic like S states, and that the last occupied band is the quadruply occupied E_g band. Note the inversion of the atomic Ti 4s and $3d^2$ states, compared to MoS_2 . All of the MO logic exposed here is valid for monolayer TMDs as well, and we find counterintuitive signs there as well, as in Sohler et al. [43].

The bonding between Mo and S is of two types: the bonding MO transfer charge from Mo to S, as expected from electronegativity and intuition. However, the last filled MO is antibonding, and transfers charge from S p orbitals to the Mo d orbitals. In chemistry this is known as π back-bonding, a process in which a σ bond is formed with the expected charge transfer, then an additional π orbital of a ligand (here the chalcogen atoms) transfers charge back to a d state of a transition metal atom [48]. This is seen in Fig. 2, the A'_1 orbital is composed of Mo 4d atomic orbitals S 3s atomic orbitals. We have shown in Table I that the static Bader charges are poor indicators of the underlying bonding characteristics of the material as they give positive charges on the metal ion, no matter the characteristics of the bonding, and they also display inconsistent behavior as a function of the atomic displacement (supplemental material [36]). The dynamic BEC sign change is a clear indicator of the subtle difference in bonding in these materials. A high-throughput screening of anomalous BEC in many more materials is ongoing.

Experimentally it will be difficult to determine the sign of the BEC as most quantities, in particular the LO - TO splitting, depend on the magnitude of the BEC and not its sign. However, since the negative BEC are a fundamental material property, they should be measurable, e.g. in a system where the mirror plane symmetry is broken. A small movement of the transition-metal ion would then lead to an asymmetric effect as a function of applied fields or strain. There exists TMD materials with similar planes to h-TMDs, but lower lattice symmetry due to stacking, in particular TcS_2 , ReS_2 , and ReSe_2 which belong to triclinic space groups. Their unit cells are more complex, with inequivalent metal sites and buckled chalcogens. We believe in these materials, and the others already mentioned, that the Raman suscep-

tibility can be used to determine the sign of the BEC. The Raman susceptibility is *linearly* dependent on the BEC [49] and can be used to deduce the sign a BEC in an angle resolved Raman measurement similar to Wolverson *et al.* [50]. Finally, it may also be possible to measure the inverted sign of the BEC using using X-ray absorption spectroscopy in a strong electric field, which is atom-specific [51]. Note that, for h-TMD in a homogeneous field of any direction, half of the bonds will be stretched and the other half compressed, making it impossible to distinguish the BEC sign.

In conclusion, we have shown that the Born Effective Charges in the hexagonal TMDs are anomalous in sign. This arises from the change in the electronic density due to an electric field perturbation, which is localized on the transition-metal ion. We have also shown that the localization of the perturbed density arises from the bonding characteristics of the molecular orbitals, in which the highest occupied orbital is anti-bonding, with strong transition-metal characteristics. Upon a displacement of either atom, the highest occupied A'_1 orbital will transfer more charge through π back bonding. The mechanism is identical in monolayers of TMDs, and in systems with hexagonal layers but broken stacking symmetry. These results are the first observation of an anomalous sign in the BEC, and confirm their powerful role in probing bonding characteristics in complex systems. The experimental determination of the sign of the BEC is an important issue, for which we make a few suggestions.

ACKNOWLEDGMENTS

We gratefully acknowledge discussions with G. Petretto and Ph. Ghosez. The authors acknowledge the Belgian Fonds National de la Recherche Scientifique FNRS under grant number PDR T.1077.15-1/7 (N.A.P and M.J.V) and for a FRIA Grant (B.V.T.). M.J.V and A.D. acknowledge support from ULg and from the Communauté Française de Belgique (ARC AIMED 15/19-09). Computational resources have been provided by the Université Catholique de Louvain (CISM/UCL); the Consortium des Equipements de Calcul Intensif en Fédération Wallonie Bruxelles (CECI), funded by FRS-FNRS G.A. 2.5020.11; the Tier-1 supercomputer of the Fédération Wallonie-Bruxelles, funded by the Walloon Region under G.A. 1117545; and by PRACE-3IP DECI grants, on ARCHER and Salomon (ThermoSpin, ACEID, OPTOGEN, and INTERPHON 3IP G.A. RI-312763).

* Nicholas.pike@ulg.ac.be

[1] M. Pumera and Z Sofer and A. Ambrosi. "Layered transition metal dichalcogenides for electrochemical energy

- generation and storage.” *J. Mater. Chem. A*, **2**, 8981-8987 (2014).
- [2] D. Jariwala and V. K. Sangwan and L. J. Lauhon and T. J. Marks and M. C. Hersam. “Emerging Device Applications for Semiconducting Two-Dimensional Transition Metal Dichalcogenides.” *ACS Nano* **8**, 1102-1120 (2014).
- [3] A. Gupta and T. Sakhivel and S. Seal. “Recent Developments in 2D materials beyond graphene.” *Prog. in Mat. Sci.* **73**, 44 - 126 (2015).
- [4] G. R. Bhimanapati and Z. Lin and V. Meunier and Y. Jung and J. Cha and S. Das and D. Xiao and Y. Son and M. S. Strano and V. R. Cooper and L. Liang and S. G. Louie and E. Ringe and W. Zhou and S. S. Kim and R. R. Naik and B. G. Sumpter and H. Terrones and F. Xia and Y. Wang and J. Zhu and D. Akinwande and N. Alem and J. A. Schuller and R. E. Schaak and M. Terrones and J. A. Robinson. “Recent Advances in Two-Dimensional Materials Beyond Graphene.” *ACS Nano* **9**, 11509-11539 (2015).
- [5] Q. H. Wang and K. Kalantar-Zadeh and A. Kis and J. N. Coleman and M. S. Strano. “Electronic and optoelectronics of two-dimensional transition metal dichalcogenides.” *Nature Nanotechnology* **7**, 699-712 (2012).
- [6] C. Espejo and T. Rangel and A. H. Romero and X. Gonze and G.-M. Rignanese. “Band structure tunability in MoS₂ under interlayer compression: a DFT and GW study.” *Phys. Rev. B* **87**, 245114 (2013).
- [7] B. Radisavljevic and A. Radenovic and J. Brivio and V. Giacometti and A. Kis. “Single-layer MoS₂ Transistors.” *Nature Nanotechnology* **6**, 147-150 (2011).
- [8] N. Kumar and S. Najmaei and Q. Cui and F. Ceballos and P. M. Ajayan and J. Lou and H. Zhao. “Second Harmonic microscopy of monolayer MoS₂.” *Phys. Rev. B* **87**, 161403(R) (2013).
- [9] A. Kuc and T. Heine and A. Kis. “Electronic Properties of transition-metal dichalcogenides.” *MRS Bulletin* **40** 577-584 (2015).
- [10] L. Tao and E. Cinquanta and D. Chiappe and C. Grazianetti and M. Faniculli and M. Dubey and A. Molle and D. Akinwande. “Silicene field-effect transistors operating at room temperature.” *Nature Nanotechnology* **10**, 227-231 (2015).
- [11] M. E. Davila and L. Xian and S. Cahangirov and A. Rubio and G. Le Lay. “Germanene: a novel two-dimensional germanium allotrope akin to graphene and silicene.” *New. J. of Phys.* **16**, 095002 (2014).
- [12] R. M. White and G. Lucovsky. “Chemical Bonding and Structure in Layered Transition Metal Dichalcogenides.” *Solid. State. Communications* **11**, 1369- 1373 (1972).
- [13] G. Lucovsky and R. M. White and J. A. Benda and J. F. Revelli. “Infrared-Reflectance Spectra of Layered Group -IV and Group-VI Transition-Metal Dichalcogenides.” *Phys. Rev. B* **7**, 3859 (1973).
- [14] J.-Q. Li and D.-P. Huang. “The energy band structures and chemical bonds of solid state compounds with low-dimensional structures. Part I: Delocalized $d - p\pi$ bonding and conductivity of transition metal compounds with low-dimensional structures.” *J. Mol. Struct. (Theochem)* **363**, 23-33 (1996).
- [15] C. M. Fang and R. A. de Groot and C. Haas. “Bulk and surface electronic structure of 1T- TiS₂ and 1T-TiSe₂.” *Phys. Rev. B* **56**, 4455 (1997).
- [16] Y. -H. Liu and S. H. Porter and J. E. Goldberger. “Dimensional Reduction of a Layered Metal Chalcogenide into a 1D Near-IR Direct Band Gap Semiconductor.” *J. Am. Chem. Soc.* **134**, 5044-5047 (2012).
- [17] S. Sharma and T. Nautiyal and G. S. Singh and S. Auluck and P. Blaha and C. Ambrosh-Draxl. “Electronic Structure of 1T-TiS₂.” *Phys. Rev. B* **59**, 14833 (1999).
- [18] R. M. Martin *Electronic Structure: Basic Theory and Practice Methods*. Cambridge University Press, (2004).
- [19] R. F. W. Bader. “Atoms in Molecules.” *Acc. Chem. Res.* **18**, 9-15 (1985).
- [20] F. L. Hirshfeld. “Bonded-atom fragments for describing molecular charge densities.” *Theoret. Chim. Acta.* **44**, 129-138 (1977).
- [21] Ph. Ghosez and J-P. Michenaud and X. Gonze. “Dynamical atomic charges: The case of ABO₃ compounds.” *Phys. Rev. B* **58**, 6224 (1998).
- [22] X. Gonze. “First-principles responses of solids to atomic displacements and homogeneous electric fields: Implementation of a conjugate-gradient algorithm.” *Phys. Rev. B* **55**, 10337 (1997).
- [23] X. Gonze and G.-M. Rignanese and M. Verstraete and J.-M. Beuken and Y. Pouillon and R. Caracas and F. Jollet and M. Torrent and G. Zerah and M. Mikami and Ph. Ghosez and M. Veithen and J.-Y. Raty and V. Olevano and F. Bruneval and L. Reining and R. Godby and G. Onida and D.R. Hamann and D.C. Allan. “A brief introduction to the ABINIT software package.” *Z. Kristallogr.* **220**, 558-562 (2005).
- [24] X. Gonze and B. Amadon and P. M. Anglade and J.-M. Beuken and F. Bottin and P. Boulanger and F. Bruneval and D. Caliste and R. Caracas and M. Cote and T. Deutsch and L. Genovese and Ph. Ghosez and M. Giantomassi and S. Goedecker and D. Hamann and P. Hermet and F. Jollet and G. Jomard and S. Leroux and M. Mancini and S. Mazevet and M.J.T. Oliveira and G. Onida and Y. Pouillon and T. Rangel and G.-M. Rignanese and D. Sangalli and R. Shaltaf and M. Torrent and M.J. Verstraete and G. Zerah and J.W. Zwanziger. “ABINIT : first-principles approach to material and nanosystem properties.” *Comput. Phys. Commun.* **180**, 2582-2615 (2009).
- [25] X. Gonze and F. Jollet and F. Abreu Araujo and D. Adams and B. Amadon and T. Applencourt and C. Audouze and J.-M. Beuken and J. Bieder and A. Bokhanchuk and E. Bousquet and F. Bruneval and D. Caliste and M. Cote and F. Dahm and F. Da Pieve and M. Delaveau and M. Di Gennaro and B. Dorado and C. Espejo and G. Geneste and L. Genovese and A. Gerossier and M. Giantomassi and Y. Gillet and D.R. Hamann and L. He and G. Jomard and J. L. Janssen and S. Le Roux and A. Levitt and A. Lherbier and F. Liu and I. Lukacevic and A. Martin and C. Martins and M.J.T. Oliveira and S. Ponce and Y. Pouillon and T. Rangel and G.-M. Rignanese and A.H. Romero and B. Rousseau and O. Rubel and A.A. Shukri and M. Stankovski and M. Torrent and M.J. VanSetten and B. Van Troeye and M.J. Verstraete and D. Waroquiers and J. Wiktorski and B. Xu and A. Zhou and J.W. Zwanziger. “Recent developments in the ABINIT software package.” *Comput. Phys. Commun.* **205**, 106-131 (2016).
- [26] J. P. Perdew and K. Burke and M. Ernzerhof, “Generalized Gradient Approximation Made Simple.” *Phys. Rev. Lett.* **77**, 2865 (1996).
- [27] M. Fuchs and M. Scheffler. “Ab initio pseudopotentials for electronic structure calculations of poly-atomic sys-

- tems using density-functional theory.” *Comput. Phys. Commun.* **119**, 67 (1999).
- [28] B. Van Troeye and M. Torrent and X. Gonze. “Interatomic force constants including the DFT-D dispersion contribution.” *Phys. Rev. B* **93**, 144304 (2016).
- [29] S. Grimme and S. Ehrlich and L. Goerigk. “A consistent and accurate ab-initio parametrization of density functional dispersion correction (DFT-D) for the 94 elements H-Pu.” *J. Chem. Phys.* **132**, 154104 (2010).
- [30] R. Dickinson and L. Pauling. “The crystal Structure of Molybdenite.” *J. Amer. Chem. Soc.* **45**, 1466-1471 (1923).
- [31] L. H. Brixner. “Preparation and properties of the single crystalline AB₂-type selenides and tellurides of niobium, tantalum, molybdenum and tungsten.” *J. Inorg. Nucl. Chem.* **24**, (1962).
- [32] A. Berkdemir and H. R. Guterrez and A. R. Botello-Mendez and N. Perea-Lopez and A. L. Elias and C-I. Chia and V. H. Crespi and F. Lopez-Urias and J-C. Charlier and H. Terrones and M. Terrones. “Identification of individual and few layers of WS₂ using Raman Spectroscopy.” *Sci. Repts.* **3**, 1755 (2013).
- [33] M. Traving and M. Boehme and L. Kipp and M. Skibowski and F. Starrost and E. E. Krosovskii and A. Perlov and W. Schattke. “Electronic Structure of WSe₂: A combined photoemission and inverse photoemission study.” *Phys. Rev. B* **55**, 10392 (1997).
- [34] C. Wan and Y. Wang and N. Wang and K. Koumoto. “Low-Thermal-Conductivity $(MS)_{1+x}(TiS_2)_2$ (M = Pb, Bi, Sn) Misfit layer Compounds for Bulk Thermoelectrics.” *Materials* **3**, (2010).
- [35] P. Chen and Y-H. Chan and X-Y. Fang and Y. Zhang and M. Y. Chou and S-K. Mo and Z. Hussain and A. V. Fedorov and T. C. Chaing. “Charge density wave transition in single-layer titanium diselenide. *Nature Communications*. **6**, 8943 (2015).
- [36] See supplemental material for additional details [8, 21, 24, 26, 27, 29–35, 37, 49, 50]
- [37] X. Gonze and C. Lee. “Dynamical matrices, Born effective charges, dielectric permittivity tensors, and interatomic force constants from density-functional perturbation theory.” *Phys. Rev. B* **55**, 10355 (1997).
- [38] S. Baroni and S. de Gironcoli and A. Dal Corso and P. Giannozzi. “Phonons and related crystal properties from density-functional perturbation theory.” *Rev. Mod. Phys.* **73**, 515 (2001).
- [39] Q.-C. Sun and X. S. Xu and L. I. Vergara and R. Rosentsveig and J. L. Musfeldt. “Dynamical charge and structural strain in inorganic fullerene-like MoS₂ nanoparticles.” *Phys. Rev. B* **79**, 205405 (2009).
- [40] T. J. Wieting and A. Grisel and F. Levy. “Interlayer Bonding and Localized Charge in MoSe₂ and α -MoTe₂.” *Physica B* **99**, 337-342 (1980).
- [41] R. D. Luttrell and S. Brown and J. Cao and J. L. Musfeldt and R. Rosentsveig and R. Tenne. “Dynamics of bulk versus nanoscale: WS₂: Local strain and charging effects.” *Phys. Rev. B* **73**, 035410 (2006).
- [42] S. -I. Uchida and S. Tanaka. “Optical Phonon Modes and Localized Effective Charges of Transition-Metal Dichalcogenides.” *J. Phys. Soc. Jpn.* **45**, 153- 191 (1978).
- [43] T. Sohler and M. Calandra and F. Mauri. “Two-dimensional Frohlich interaction in transition-metal-dichalcogenide monolayers: theoretical modeling and first-principle calculations.” *Phys. Rev. B* **94**, 085415 (2016).
- [44] Ph. Ghosez and X. Gonze. “Band-by-band decompositions of the Born effective charges.” *J. of Phys.: Condens. Mat.* **12**, 9179 (2000).
- [45] M. Veithen and X. Gonze and Ph. Ghosez. “Electron localization: Band-by-band decomposition and application to oxides.” *Phys. Rev. B* **66**, 235113 (2002).
- [46] P. D. Fleischauer and J. R. Lince and P. A. Bertrand and R. Bauer. “Electronic Structure and Lubrication Properties of MoS₂: A Qualitative Molecular Orbital Approach.” *Langmuir* **5**, 1009-1015 (1989).
- [47] E. I. Stiefel and R. Eisenberg and R. C. Rosenberg and H. B. Gray. “Characterization and Electronic Structure of Six-Coordinate Trigonal-Prismatic Complexes.” *J. Am. Chem. Soc.* **88**, 2956-2966 (1966).
- [48] G. L. Meissler and P. J. Fischer and D. A. Tarr. *Inorganic Chemistry* 5th edition. Pearson (2014).
- [49] M. Veithen and X. Gonze and Ph. Ghosez. “Non-linear optical susceptibilities, Raman efficiencies and electrooptic tensors from first-principles density functional perturbation theory.” *Phys. Rev. B* **71**, 125107 (2005).
- [50] D. Wolverson and S. Crampin, and A. S. Kazemi, and A. Ilie and S. J. Bending. “Raman Spectra of Monolayer, Few-Layer and Bulk ReSe₂: An Anisotropic Layered Semiconductor.” *ACSNANO* **8**, 11154-11164 (2014).
- [51] V. Ney and W. K. Ollefs and A. Rogalev and A. Ney. “X-ray absorption spectroscopy in electrical fields: An element-selective probe of atomic polarization.” *Phys. Rev. B* **93**, 035136 (2016).